Influence of an extended source on Goniopolarimetry (or Direction Finding) with Cassini and STEREO radio receivers

B. Cecconi

Oct. 23rd, 2006: Accepted for Publication in Radio Science (AGU)

Abstract

In a recent paper, Cecconi and Zarka (2005) provided analytical goniopolarimetric inversions — i.e. which allow us to retrieve the direction of arrival of an incoming electromagnetic wave, its flux, and its polarization state, also referred as direction finding inversions — to be used with measurements acquired with a system of electric dipole antennas on a three axis stabilized spacecraft such as the Cassini/RPWS/HFR or the STEREO/Waves receivers. In the present study, we establish the expressions of the measurements (auto- and cross-correlations) in the case of an extended source . We also analyze the effect of an extended source on the outputs of the analytical inversions presented in the former paper, which are supposing a point radio source. We show that for a source with an angular half width smaller than 5°, the induced biases are not significant.

1 Introduction

As the Earth's ionosphere is reflecting out incoming low frequency radio waves, space based radio experiments are necessary in the range $f \leq 10\,MHz$. Constraints on size and mass of embarked antennas impose the use of simple antennas (monopoles or dipoles) of typical length $L \sim 10 - 50\,m$. The corresponding spatial resolution of such radio instruments — defined as λ/D, where λ is the observation wavelength and D the typical aperture of the telescope or radio telescope — is very poor, as $\lambda/L \sim 1$ or even $\gg 1$. There is thus no instantaneous spatial resolution with such antennas. A more adapted description of the antenna directivity is its beaming pattern which gives the antenna gain for each direction of space. The beaming pattern of a short dipole — the short dipole approximation requires $L \ll \lambda$ — varies as $\sin^2\theta$ where θ is the angular distance between the source direction and the dipole direction. By integration of the beaming pattern over the whole space, we get the beaming solid angle, which is $8\pi/3\,sr$ for a short dipole. This solid angle represents thus $2/3$ of the 4π sphere. Specific techniques have been derived to retrieve angular resolution from measurements performed simultaneously with several (2 or 3) dipoles: these are named Direction–Finding techniques in the literature. As the determination of the wave vector $\vec{k}$ (direction of arrival of the wave) is coupled with the determination of the wave polarization (e.g. 2 waves with opposite circular polarization and coming from opposite directions give the same signature), I propose to use instead the word Goniopolarimetry (GP), which recalls that we get both direction and polarization of the incoming wave.

Available GP techniques include (i) analysis of the modulations of the signal received by 1 or 2 antennas on a spinning spacecraft [*Lecacheux*, 1978; *Manning and Fainberg*, 1980; *Ladreiter et al.*, 1994]; (ii) analysis of auto- and cross-correlations measured on 2 or 3 antennas on a 3 axis stabilized spacecraft [*Lecacheux*, 1978; *Ladreiter et al.*, 1995; *Vogl et al.*, 2004; *Cecconi and Zarka*, 2005].

Cecconi and Zarka [2005] (hereafter paper 1) presented a new set of analytical GP techniques, adapted to the RPWS (Radio and Plasma Wave Science) experiment onboard Cassini [*Gurnett et al.*, 2004]. Due to similarity in the receiver design, these same inversion techniques will be used for analysing the data collected by the radio receivers (Waves) of the two STEREO (Solar TErrestrial RElations Observatory) spacecrafts [*Kaiser*, 2005].

The GP techniques presented in paper 1 are based on the assumption that the radio source is unresolved. A radio source is considered unresolved when its apparent size is smaller than the spatial resolution of the observing system. In paper 1, we showed that the derived source position accuracy is of the order of $1 - 2^\circ$ for point source GP. This accuracy is suitable for the Cassini data measured at Saturn, but is insufficient for STEREO data, as the solar radio bursts have a broad extension as viewed from the orbit of the Earth [*Steinberg et al.*, 1985]. The purpose of this paper is to take into account extended sources. In addition to the wave flux density (I), polarization (Q, U, V) and direction of arrival (θ, ϕ), we add here one parameter: the disk-equivalent radius of the source, which is the radius of the disk-like equivalent source best representing the real source (the latter being not necessarily a disk). We propose three source modelizations defined by their radial intensity profile: uniform, spherical or gaussian. Any other intensity profile can be studied numerically.

We evaluate the analytical expressions of the measurements (auto- and cross-correlations) including the angular extension of the source. We also investigate the effect of the source extension on goniopolarimetric results using point source inversions.

2 Correlation Response to an Extended Source

The analysis below is inspired by *Manning and Fainberg* [1980], who proposed inversions for Ulysses/URAP measurements (spinning spacecraft with a system of two orthogonal antennas, but without cross correlation measurements). We extend here their study to radio measurements obtained on a stabilized spacecraft with a system of antenna with any geometrical configuration. We consider an extended source subtending a solid angle Ω. All the directions are specified by their colatitude θ and azimuth ϕ. As we express the typical extension of the source in terms of its disk-equivalent radius, we will consider an axisymmetric equivalent source and centered on the (θ_C, ϕ_C) direction. The angular disk-equivalent radius is γ so that $\Omega = 2\pi(1 - \cos\gamma)$. Any point M of the source is defined by its (θ_M, ϕ_M) direction. Fig. 1 illustrates these definitions in an adequate coordinate system. All points of the source are considered to have the same polarization Stokes parameters (Q, U, V) [*Kraus*, 1966] (homogeneous source assumption), but we allow a radial flux density S profile. We also consider that the electromagnetic waves coming from each point of the source is phase-decorrelated with the waves coming from the neighboring points of the source (phase-decorrelation assumption).

We consider valid the short antenna hypothesis, i.e. the equivalent dipole effective lengths (L) are short compared to the wavelength, i.e. $L \ll \lambda$. The effective length of the Cassini/RPWS electrical antennas is $8.5\,m$ in dipole mode and $7.9\,m$ in monopole mode [*Zarka et al.*, 2004], which gives an upper frequency limit $\sim 1.5\,MHz$ for the validity of the GP analysis. For the STEREO/Waves antennas, the equivalent dipole effective lengths have not been measured in-flight at the time of this writing, but *Oswald et al.* [2006] and *Rucker et al.* [2005] estimated through wire-grid simulations that the upper frequency limit for GP is about $\sim 1.5\,MHz$ (and stressed upon the need for confirmation by in-flight calibration). The physical antenna length is $6\,m$. Below $1.5\,MHz$, we can thus assume that each electrical antenna — composed of a monopole and the spacecraft's conducting body — is equivalent to a perfect dipole, whose effective parameters (length (h) and direction (θ, ϕ)) must be carefully calibrated before GP analysis [*Vogl et al.*, 2004,paper 1]. Under this assumption, the voltage V measured at the antenna's output is the projection of the wave electric field $\vec{E}$ on the effective electrical antenna $\vec{h}$, i.e. $V = \vec{h}.\vec{E}$. For an electromagnetic waves, the electric field is

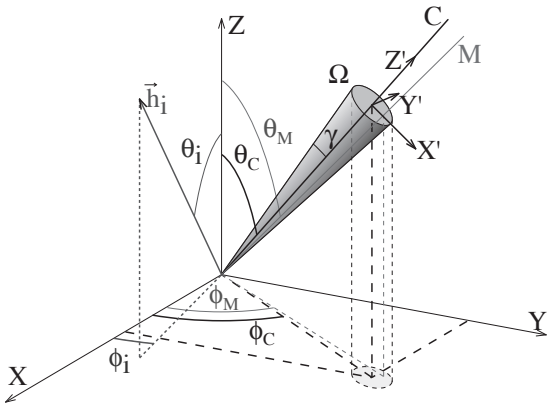

Figure 1: Coordinate system adapted to an axisymmetric source of half viewing angle γ, and centered in direction C (at colatitude θ_C and azimuth ϕ_C). M is the direction of one point of the source. $\vec{h}_i$ is the direction of the ith antenna. The (X, Y, Z) frame is the spacecraft frame. We also represented the source center reference frame axes (X', Y', Z'), which is defined is section 2.2.

represented by a canonical complex function of time: $\vec{E} = \vec{E}_0 \exp(i\omega t)$, where ω is the wave pulsation. The instantaneous voltage at the antenna's output is then $V = \vec{E}_0.\vec{h} \exp(i\omega t)$.

The measurement P_{ij} is the voltage correlation between the antenna i and j outputs and writes $P_{ij} = \langle V_i V_j^* \rangle$, where V_i and V_j are the voltages measured at antenna i and j outputs respectively, V^* is the complex conjugate of V, and $\langle \cdots \rangle$ denotes the averaging over an integration time longer than the wave period. If $i = j$, P_{ii} is the autocorrelation of voltages on antenna i, hence a power; if $i \neq j$, P_{ij} is a cross-correlation.

2.1 Phase-decorrelated source

In the case of point source GP, the expression of the correlation P_{ij} was derived in *Ladreiter et al.* [1995] and paper 1. Including explicitly the impedance of free space Z_0 and the antenna system gain Gh_ih_j [*Manning*, 2000] into P_{ij}, we obtain:

$$P_{ij} = Z_0\, G h_i h_j\, S_{ij} \tag{1}$$

with:

$$S_{ij} = \frac{S}{2}\big[(1+Q)\Omega_i\Omega_j + (1-Q)\Psi_i\Psi_j + (U-iV)\Omega_i\Psi_j + (U+iV)\Omega_j\Psi_i\big] \tag{2}$$

where $\Omega_n = (\vec{h}_n.\vec{X}_w)/h_n$ and $\Psi_n = (\vec{h}_n.\vec{Y}_w)/h_n$ are the coordinates of the nth antenna unit vector projected on the wave plane $(O, \vec{X}_w, \vec{Y}_w)$ [see *Ladreiter et al.*, 1995, and next section]; the Stokes parameters are: the source flux density S (in $W\,m^{-2}\,Hz^{-1}$), the linear polarization degrees Q and U, and the circular polarization degree V. Note that we use the fractional definition of the Stokes parameter polarization degrees — i.e. the total received power with e.g. pure circular polarization corresponds to the product $S \times V$. The expressions of Ω_n and Ψ_n are valid in any reference frame.

In order to study the case of an extended source, we suppose that the source is spatially phase-decorrelated, i.e. that wave packets emitted by each point of the source is phase-decorrelated to the wave packets from every other point of the source. The correlation P_{ij} then becomes:

$$P_{ij} = \int_\Omega dP_{ij} \tag{3}$$

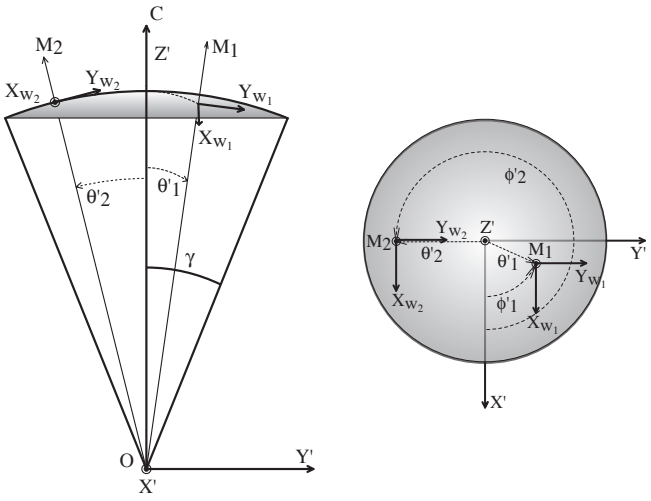

(a) (b)

Figure 2: Reference frame for en extended source: (a) projection on the $(OY'Z')$ plane, (b) polar view. The extended source reference frame (X', Y', Z') is defined such that the Z' axis points towards the center C of the extended source. The M_1 and M_2 directions point to two elementary sources in the extended source. γ is the angular half aperture of the source, as seen by an observer placed at the origin O of the frame. The X_{w_i} and Y_{w_i} unit vectors are in the wave plane, perpendicular to the M_i direction (as defined in section 2.2).

with:

$$dP_{ij} = \frac{\partial P_{ij}}{\partial \Omega} d\Omega = P_{ij}^{\Omega} d\Omega = Z_0 \, G h_i h_j \, S_{ij}^{\Omega} \, d\Omega \tag{4}$$

and:

$$S_{ij}^{\Omega} = \frac{S^{\Omega}}{2} \left[(1+Q)\Omega_i \Omega_j + (1-Q)\Psi_i \Psi_j + (U - iV)\Omega_i \Psi_j + (U + iV)\Omega_j \Psi_i \right] \tag{5}$$

where S^{Ω} is the brightness distribution (in $W m^{-2} \, Hz^{-1} \, sr^{-1}$) over the source. At this point, there is no assumption on source homogeneity, i.e. S^{Ω}, Q, U and V may change across the source.

2.2 Source center frame

We name (X, Y, Z) the spacecraft coordinate system. The source center frame (X', Y', Z') is defined as follows: Z' is pointing towards the center of the source; X' is in the (Z, Z') plane and its colatitude in the (X, Y, Z) frame is $\theta_C + \pi/2$; $Y' = Z' \times X'$. In this frame, the angles defining the directions of a point M of the source are the colatitude θ'_M and the azimuth ϕ'_M. The transformation matrix from (X', Y', Z') to (X, Y, Z) is:

$$\begin{pmatrix} X \\ Y \\ Z \end{pmatrix} = \begin{pmatrix} \cos\theta_C \cos\phi_C & -\sin\phi_C & \sin\theta_C \cos\phi_C \\ \cos\theta_C \sin\phi_C & \cos\phi_C & \sin\theta_C \sin\phi_C \\ -\sin\theta_C & 0 & \cos\theta_C \end{pmatrix} \begin{pmatrix} X' \\ Y' \\ Z' \end{pmatrix} \tag{6}$$

Here, X' and Y' orientation has been defined univocally from the spacecraft coordinate system. These vectors can also be defined using specific axes related to the studied source. The transformation matrix is then different but the results derived remain identical.

For each elementary source M_i, the vectors $\vec{X}_{w_i}$ and $\vec{Y}_{w_i}$ define the wave plane. There is no theoretical constraint on the orientation of this pair of vectors, as far as they remain perpendicular to each other [see

Ladreiter et al., 1995; *Manning and Fainberg*, 1980]. The wave frame orientation defines the directions of the linear polarization axes. Thus, in order for the linear polarization degrees (Stokes parameters Q and U) to be consistent over a series of observations from various directions in space, the wave frame orientation should not rotate throughout the source. In the case of an extended source, made of elementary sources M_i, the wave frame must be defined so that all the $\vec{X}_{w_i}$ vectors are parallel to each other and all the $\vec{Y}_{w_i}$ vectors are also parallel to each other. As waves planes are not parallel across the extended source — i.e. the source directions $\vec{Z}_{w_i}$ are not colinear — we must to relax the latter constraint: the projections of the vectors $\vec{Y}_{w_i}$ on the $(OX'Y')$ plane — perpendicular to the source center direction — must be parallel as viewed from the observer. This condition is illustrated in Fig. 2.

The wave frame vectors in the source center frame (X', Y', Z'), $\vec{X}'_{w_i}(\theta'_i, \phi'_i)$, $\vec{Y}'_{w_i}(\theta'_i, \phi'_i)$ and $\vec{Z}'_{w_i}(\theta'_i, \phi'_i)$, depend on θ'_i and ϕ'_i. The above condition on the wave frame orientation should then be fulfilled in the vicinity of the Z' axis, which is the direction of the source center. In *Ladreiter et al.* [1995] this condition is not fulfilled, whereas it is in *Manning and Fainberg* [1980]. We will thus use the latter definition. We also use a reference vector named $\vec{Y}_0$, in order to define the wave frame orientation. The wave frame vectors are then defined as follows:

$$\vec{Z}'_w = \begin{pmatrix} \sin\theta'_M \cos\phi'_M \\ \sin\theta'_M \sin\phi'_M \\ \cos\theta'_M \end{pmatrix} \tag{7}$$

$$\vec{Y}'_w = \frac{\vec{Z}'_w \times (\vec{Y}_0 \times \vec{Z}'_w)}{||\vec{Y}_0 \times \vec{Z}'_w||} \tag{8}$$

$$\vec{X}'_w = \vec{Y}'_w \times \vec{Z}'_w \tag{9}$$

Equation (7) means that $\vec{Z}'_w$ points to the source M. Equation (8) defines a unit vector perpendicular to the line of sight within the $(\vec{Y}_0, \vec{Z}'_w)$ plane. As equation (8) is only valid if $\vec{Y}_0$ and $\vec{Z}'_w$ are not colinear, the orientation of $\vec{Y}_0$ has to be carefully chosen depending on the source direction and on the object studied: in the case of planetary radio emissions, the vector $\vec{Y}_0$ can be defined as the orientation of the magnetic axis of the studied planet; for solar corona radio bursts, $\vec{Y}_0$ can be taken perpendicular to the ecliptic plane.

For the ease of further computation, we choose $\vec{Y}_0 = \vec{Y}'$, as in *Manning and Fainberg* [1980]. Then:

$$\vec{X}'_w = \frac{1}{\sqrt{1 - \sin^2\theta'_M \sin^2\phi'_M}} \begin{pmatrix} \cos\theta'_M \\ 0 \\ -\sin\theta'_M \cos\phi'_M \end{pmatrix} \tag{10}$$

$$\vec{Y}'_w = \frac{1}{\sqrt{1 - \sin^2\theta'_M \sin^2\phi'_M}} \begin{pmatrix} -\sin^2\theta'_M \cos\phi'_M \sin\phi'_M \\ 1 - \sin^2\theta'_M \sin^2\phi'_M \\ -\sin\theta'_M \cos\theta'_M \sin\phi'_M \end{pmatrix} \tag{11}$$

Going back in the spacecraft frame (X, Y, Z) using equation (6), we obtain:

$$\vec{X}_w = \frac{1}{\sqrt{1 - \sin^2\theta'_M \sin^2\phi'_M}} \begin{pmatrix} \cos\theta_C \cos\phi_C \cos\theta'_M - \sin\theta_C \cos\phi_C \sin\theta'_M \cos\phi'_M \\ \cos\theta_C \sin\phi_C \cos\theta'_M - \sin\theta_C \sin\phi_C \sin\theta'_M \cos\phi'_M \\ -\sin\theta_C \cos\theta'_M - \cos\theta_C \sin\theta'_M \cos\phi'_M \end{pmatrix} \tag{12}$$

$$\vec{Y}_w = \frac{1}{\sqrt{1 - \sin^2\theta'_M \sin^2\phi'_M}} \times$$

$$\begin{pmatrix} -\cos\theta_C \cos\phi_C \sin^2\theta'_M \cos\phi'_M \sin\phi'_M - \sin\phi_C(1 - \sin^2\theta'_M \sin^2\phi'_M) - \sin\theta_C \cos\phi_C \sin\theta'_M \cos\theta'_M \sin\phi'_M \\ -\cos\theta_C \sin\phi_C \sin^2\theta'_M \cos\phi'_M \sin\phi'_M + \cos\phi_C(1 - \sin^2\theta'_M \sin^2\phi'_M) - \sin\theta_C \sin\phi_C \sin\theta'_M \cos\theta'_M \sin\phi'_M \\ +\sin\theta_C \sin\phi_C \sin^2\theta'_M \cos\phi'_M \sin\phi'_M - \cos\theta_C \sin\theta'_M \cos\theta'_M \sin\phi'_M \end{pmatrix} \tag{13}$$

Expressions of $\Omega_i = (\vec{h}_i.\vec{X}_w)/h_i$ and $\Psi_i = (\vec{h}_i.\vec{Y}_w)/h_i$ are thus:

$$\begin{aligned}
\Omega_i &= \frac{1}{\sqrt{1-\sin^2\theta'_M\sin^2\phi'_M}}\Big[\cos\theta'_M\big(\sin\theta_C\cos\theta_i - \sin\theta_i\cos\theta_C\cos(\phi_C-\phi_i)\big) \\
&\quad -\sin\theta'_M\cos\phi'_M\big(\cos\theta_C\cos\theta_i + \sin\theta_i\sin\theta_C\cos(\phi_C-\phi_i)\big)\Big] \qquad (14)\\
\Psi_i &= \frac{1}{\sqrt{1-\sin^2\theta'_M\sin^2\phi'_M}}\Big[-(1-\sin^2\theta'_M\sin^2\phi'_M)\sin\theta_i\sin(\phi_C-\phi_i) \\
&\quad +\sin^2\theta'_M\cos\phi'_M\sin\phi'_M\big(\cos\theta_i\sin\theta_C - \sin\theta_i\cos\theta_C\cos(\phi_C-\phi_i)\big) \\
&\quad -\sin\theta'_M\cos\theta'_M\sin\phi'_M\big(\cos\theta_C\cos\theta_i + \sin\theta_i\sin\theta_C\cos(\phi_C-\phi_i)\big)\Big] \qquad (15)
\end{aligned}$$

2.3 Spatial integration

We define the following useful quantities:

$$\begin{aligned}
A_i(\theta_C,\phi_C) &= -\sin\theta_i\cos\theta_C\cos(\phi_C-\phi_i) + \cos\theta_i\sin\theta_C \qquad (16)\\
B_i(\theta_C,\phi_C) &= -\sin\theta_i\sin(\phi_C-\phi_i) \qquad (17)\\
C_i(\theta_C,\phi_C) &= \sin\theta_i\sin\theta_C\cos(\phi_C-\phi_i) + \cos\theta_i\cos\theta_C \qquad (18)
\end{aligned}$$

This allows us to rewrite Ω_i and Ψ_i as:

$$\begin{aligned}
\Omega_i &= \frac{A_i(\theta_C,\phi_C)\cos\theta'_M - C_i(\theta_C,\phi_C)\sin\theta'_M\cos\phi'_M}{\sqrt{1-\sin^2\theta'_M\sin^2\phi'_M}} \qquad (19)\\
\Psi_i &= \frac{1}{\sqrt{1-\sin^2\theta'_M\sin^2\phi'_M}}\big(A_i(\theta_C,\phi_C)\sin^2\theta'_M\cos\phi'_M\sin\phi'_M \\
&\quad +B_i(\theta_C,\phi_C)(1-\sin^2\theta'_M\sin^2\phi'_M) - C_i(\theta_C,\phi_C)\sin\theta'_M\cos\theta'_M\sin\phi'_M\big) \qquad (20)
\end{aligned}$$

Each term of equation (5) has then to be integrated over the extended source solid angle using the expressions Ω_i and Ψ_i given in equations (19) and (20). As the source is axisymmetric, the integrations intervals are $[0, 2\pi]$ for ϕ'_M and $[0, \gamma]$ for θ'_M, with $\gamma \leq \pi/2$. The voltage correlation P_{ij} then writes:

$$\begin{aligned}
P_{ij} &= \frac{Z_0\,G h_i h_j}{2}\int_{\phi'_M=0}^{2\pi}\int_{\theta'_M=0}^{\gamma} S^{\Omega}(\theta'_M,\phi'_M)\times \\
&\quad \Big[(1+Q)\Omega_i(\theta_C,\phi_C,\theta'_M,\phi'_M)\Omega_j(\theta_C,\phi_C,\theta'_M,\phi'_M) \\
&\quad +(U-iV)\Omega_i(\theta_C,\phi_C,\theta'_M,\phi'_M)\Psi_j(\theta_C,\phi_C,\theta'_M,\phi'_M) \\
&\quad +(U+iV)\Omega_j(\theta_C,\phi_C,\theta'_M,\phi'_M)\Psi_i(\theta_C,\phi_C,\theta'_M,\phi'_M) \\
&\quad +(1-Q)\Psi_i(\theta_C,\phi_C,\theta'_M,\phi'_M)\Psi_j(\theta_C,\phi_C,\theta'_M,\phi'_M)\Big]\sin\theta'_M d\theta'_M d\phi'_M \qquad (21)
\end{aligned}$$

As the three cases studied below have circular symmetry, integration over ϕ'_M can be performed first. Useful

integrals for this first integration step are:

$$\int_0^{2\pi} d\phi'_M = 2\pi, \tag{22}$$

$$\int_0^{2\pi} \frac{d\phi'_M}{1-\sin^2\theta'_M\sin^2\phi'_M} = 2\pi\frac{1}{\cos\theta'_M}, \tag{23}$$

$$\int_0^{2\pi} \frac{\cos\phi'_M d\phi'_M}{1-\sin^2\theta'_M\sin^2\phi'_M} = 0, \tag{24}$$

$$\int_0^{2\pi} \frac{\sin\phi'_M d\phi'_M}{1-\sin^2\theta'_M\sin^2\phi'_M} = 0, \tag{25}$$

$$\int_0^{2\pi} \frac{\cos\phi'_M\sin\phi'_M d\phi'_M}{1-\sin^2\theta'_M\sin^2\phi'_M} = 0, \tag{26}$$

$$\int_0^{2\pi} \frac{\sin 3\phi'_M d\phi'_M}{1-\sin^2\theta'_M\sin^2\phi'_M} = 0, \tag{27}$$

$$\int_0^{2\pi} \frac{\cos^2\phi'_M d\phi'_M}{1-\sin^2\theta'_M\sin^2\phi'_M} = 2\pi\frac{1-\cos\theta'_M}{\sin^2\theta'_M}, \tag{28}$$

$$\int_0^{2\pi} \frac{\cos^2\phi'_M\sin^2\phi'_M d\phi'_M}{1-\sin^2\theta'_M\sin^2\phi'_M} = 2\pi\frac{1-\cos\theta'_M-1/2\sin^2\theta'_M}{\sin^4\theta'_M} \tag{29}$$

Allowing the source brightness distribution to vary radially $S^\Omega = S^\Omega(\theta'_M)$, but assuming that the polarization state is constant all over the source, equation (21) then rewrites:

$$\begin{aligned} P_{ij} = \int_0^\gamma \frac{2\pi\, Z_0\, G h_i h_j\, S^\Omega(\theta'_M)}{2} \Big[&(1+Q)\big[(A_iA_j\cos\theta'_M + C_iC_j(1-\cos\theta'_M)\big] \\ &+(U-iV)\big[A_iB_j\cos\theta'_M\big] + (U+iV)\big[A_jB_i\cos\theta'_M\big] \\ &+(1-Q)\big[A_iA_j(1-2\cos\theta'_M+\cos^2\theta'_M)/2 + B_iB_j(1+\cos^2\theta'_M)/2 \\ &+C_iC_j(1-\cos\theta'_M)\cos\theta'_M\big]\Big]\sin\theta'_M d\theta'_M \end{aligned} \tag{30}$$

We define Γ_k as:

$$\Gamma_k = \frac{2\pi}{\Omega}\int_{\theta'_M} \frac{S^\Omega(\theta'_M)}{S_0^\Omega}\sin(k\theta'_M)d\theta'_M \tag{31}$$

with $k \in \{1,2,3\}$ and $S_0^\Omega = S^\Omega(\theta'_M = 0)$. The coefficients Γ_k are normalized by the total viewing solid angle of the source Ω in order to be independent of the size of the source. Equation (30) can be simplified using the notation Γ_k and the trigonometric identities:

$$2\cos\theta'_M\sin\theta'_M = \sin(2\theta'_M), \quad 4\cos^2\theta'_M\sin\theta'_M = \sin(3\theta'_M) + \sin\theta'_M \tag{32}$$

The correlation is finally:

$$\begin{aligned} P_{ij} = \frac{Z_0\, G h_i h_j\, S_0}{2}\Bigg[&(1+Q)\left(A_iA_j\frac{\Gamma_2}{2} + C_iC_j\left(\Gamma_1 - \frac{\Gamma_2}{2}\right)\right) \\ &+(U-iV)\left(A_iB_j\frac{\Gamma_2}{2}\right) + (U+iV)\left(A_jB_i\frac{\Gamma_2}{2}\right) \\ &+(1-Q)\left(A_iA_j\frac{1}{2}\left(\Gamma_1 - \Gamma_2 + \frac{\Gamma_3+\Gamma_1}{4}\right) + B_iB_j\frac{1}{2}\left(\Gamma_1 + \frac{\Gamma_3+\Gamma_1}{4}\right)\right. \\ &\left.+C_iC_j\left(\frac{\Gamma_2}{2} - \frac{\Gamma_3+\Gamma_1}{4}\right)\right)\Bigg] \end{aligned} \tag{33}$$

where $S_0 = S_0^\Omega\Omega$, i.e. the total flux density of an equivalent source with an uniform S_0^Ω brightness distribution, subtending a solid angle Ω.

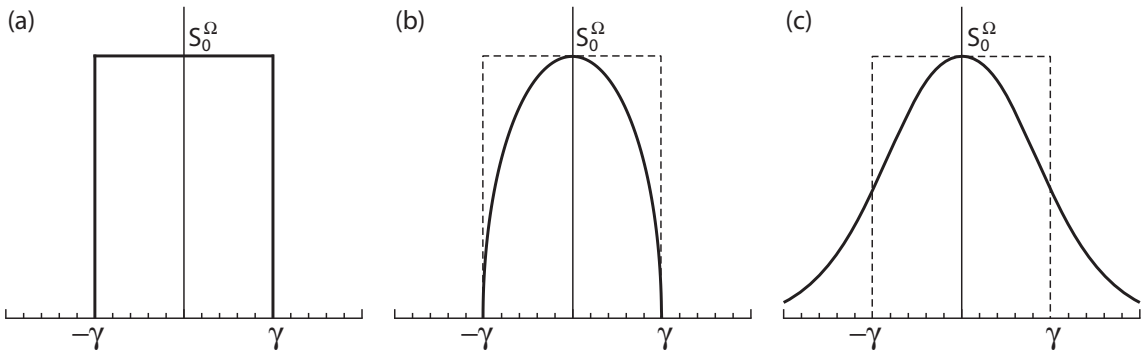

Figure 3: Radial cuts of the three source brightness distributions studied in this paper: (a) uniform source, (b) spherical source and (c) gaussian source.

2.4 Models for radial intensity profiles

We consider hereafter three models for the radial intensity source profiles, all with constant polarization (Q, U, V) across the source. The only parameter that may change across the source is the brightness distribution S^Ω, but with circular symmetry along the direction of the source center. The three cases studied (illustrated in Fig. 3) are (a) a uniform source with radius γ:

$$S_a^\Omega(\theta'_M) = S_0^\Omega, \tag{34}$$

(b) a spherical source of radius γ with an optically thin surface:

$$S_b^\Omega(\theta'_M) = K_b S_0^\Omega \sqrt{1 - \frac{\tan^2\theta'_M}{\tan^2\gamma}}, \tag{35}$$

and (c) a gaussian source with a 2γ full width at half maximum:

$$S_c^\Omega(\theta'_M) = K_c S_0^\Omega \exp(-\ln(2)\tan^2\theta'_M/\tan^2\gamma). \tag{36}$$

The coefficients K_b and K_c are normalization coefficients ensuring consistency with point source results (as described in paper 1).

2.4.1 Case of a uniform source

With a brightness profile $S_a^\Omega(\theta'_M)$ being simply S_0^Ω for $\theta'_M < \gamma$ and 0 outside, Γ_k^a is then:

$$\Gamma_k^a(\gamma) = \frac{1}{1-\cos\gamma}\int_0^\gamma \sin(k\theta'_M)d\theta'_M = \frac{1-\cos(k\gamma)}{k(1-\cos\gamma)} \tag{37}$$

for $k \in \{1,2,3\}$. Each term $\Gamma_k^a(\gamma)$ can be simplified, leading to:

$$\Gamma_1^a(\gamma) = 1, \quad \Gamma_2^a(\gamma) = 1+\cos\gamma, \quad \Gamma_3^a(\gamma) = \frac{4}{3}(1+\cos\gamma+\cos^2\gamma) - 1 \tag{38}$$

Computing the value of Γ_k^a when $\gamma \to 0$ allows us to check that the measured power is consistent with the one measured in case of a point source [*Ladreiter et al.*, 1995,paper 1]. We have:

$$\lim_{\gamma\to 0}\Gamma_k^a(\gamma) = k \tag{39}$$

This gives us the following correlation for $\gamma = 0$:

$$P_{ij} = \frac{Z_0\, G h_i h_j\, S_0}{2}[(1+Q)A_iA_j + (U-iV)A_iB_j + (U+iV)A_jB_i + (1-Q)B_iB_j] \tag{40}$$

As $A_i(\theta_C, \phi_C) = \Omega_i(\theta_C, \phi_C, 0, 0)$ and $B_i(\theta_C, \phi_C) = \Psi_j(\theta_C, \phi_C, 0, 0)$, equation (40) is exactly the expression of the measurement induced by a point source located along the (θ_C, ϕ_C) direction, with Stokes parameters S_0, Q, U, V.

2.4.2 Case of a spherical source with an optically thin surface

The brightness profile is varying radially as $S_b^\Omega(\theta'_M)$ given by equation (35). Γ_k^b then writes:

$$\Gamma_k^b(\gamma) = \frac{K_b}{1-\cos\gamma}\int_0^\gamma \left(1 - \frac{\tan^2\theta'_M}{\tan^2\gamma}\right)^{1/2} \sin(k\theta'_M)d\theta'_M \tag{41}$$

When the source is small ($\gamma \ll \pi/2$), we have $\tan(\gamma) \sim \gamma$. As $0 < \theta'_M < \gamma$, we also have $\tan\theta'_M \sim \theta'_M$ and $\sin(k\theta'_M) \sim k\theta'_M$. It is then easy to show that at the point source limit ($\gamma \to 0$), Γ_k^b becomes:

$$\lim_{\gamma\to 0}\Gamma_k^b(\gamma) = \frac{3kK_b}{2} \tag{42}$$

Setting $K_b = 2/3$, we ensure consistency with the uniform source model (a) and the limit case of a point source.

2.4.3 Case of a gaussian source

We consider here a source that has a gaussian brightness radial profile $S_c^\Omega(\theta'_M)$ given by equation (36). Γ_k^c is then:

$$\Gamma_k^c(\gamma) = \frac{K_c}{1-\cos\gamma}\int_0^{\pi/2} \exp\left(-\ln(2)\frac{\tan^2\theta'_M}{\tan^2\gamma}\right)\sin(k\theta'_M)d\theta'_M \tag{43}$$

When the source is small ($\gamma \ll \pi/2$), we have $\tan(\gamma) \sim \gamma$. The same approximation applies to $\tan\theta'_M$ only when $0 < \theta'_M < \gamma$. However, we use here this approximation from 0 to $\pi/2$, but inside an exponential function. Fig. 4 shows that this approximation is valid for all sizes of sources. Γ_k^c then rewrites:

$$\Gamma_k^c(\gamma) = \frac{K_c}{1-\cos\gamma}\int_0^{\pi/2} \exp\left(-\frac{{\theta'_M}^2}{\xi^2}\right)\sin(k\theta'_M)d\theta'_M \tag{44}$$

with $\xi = \gamma(\ln 2)^{-1/2}$ and $k \in \{1, 2, 3\}$. The limit of Γ_k^c when $\gamma \to 0$ is:

$$\lim_{\gamma\to 0}\Gamma_k^c(\gamma) = \frac{kK_c}{\ln 2} \tag{45}$$

Setting $K_c = \ln 2$, we ensure consistency with the uniform source model (a) and the limit case of a point source.

We can redefine the coefficients $\Gamma_k^b(\gamma)$ and $\Gamma_k^c(\gamma)$ including the above multiplying factors. We will thus use:

$$\Gamma_k^b(\gamma) = \frac{2}{3}\frac{1}{1-\cos\gamma}\int_0^\gamma S_b^\Omega(\theta'_M)\sin(k\theta'_M)d\theta'_M \tag{46}$$

$$\Gamma_k^c(\gamma) = \frac{\ln 2}{1-\cos\gamma}\int_0^\gamma S_c^\Omega(\theta'_M)\sin(k\theta'_M)d\theta'_M. \tag{47}$$

The numerical values for coefficients $\Gamma_k^m(\gamma)$ (with or without the small source approximation in models (b) and (c)), computed using a Romberg integration method, are shown in Fig. 4.

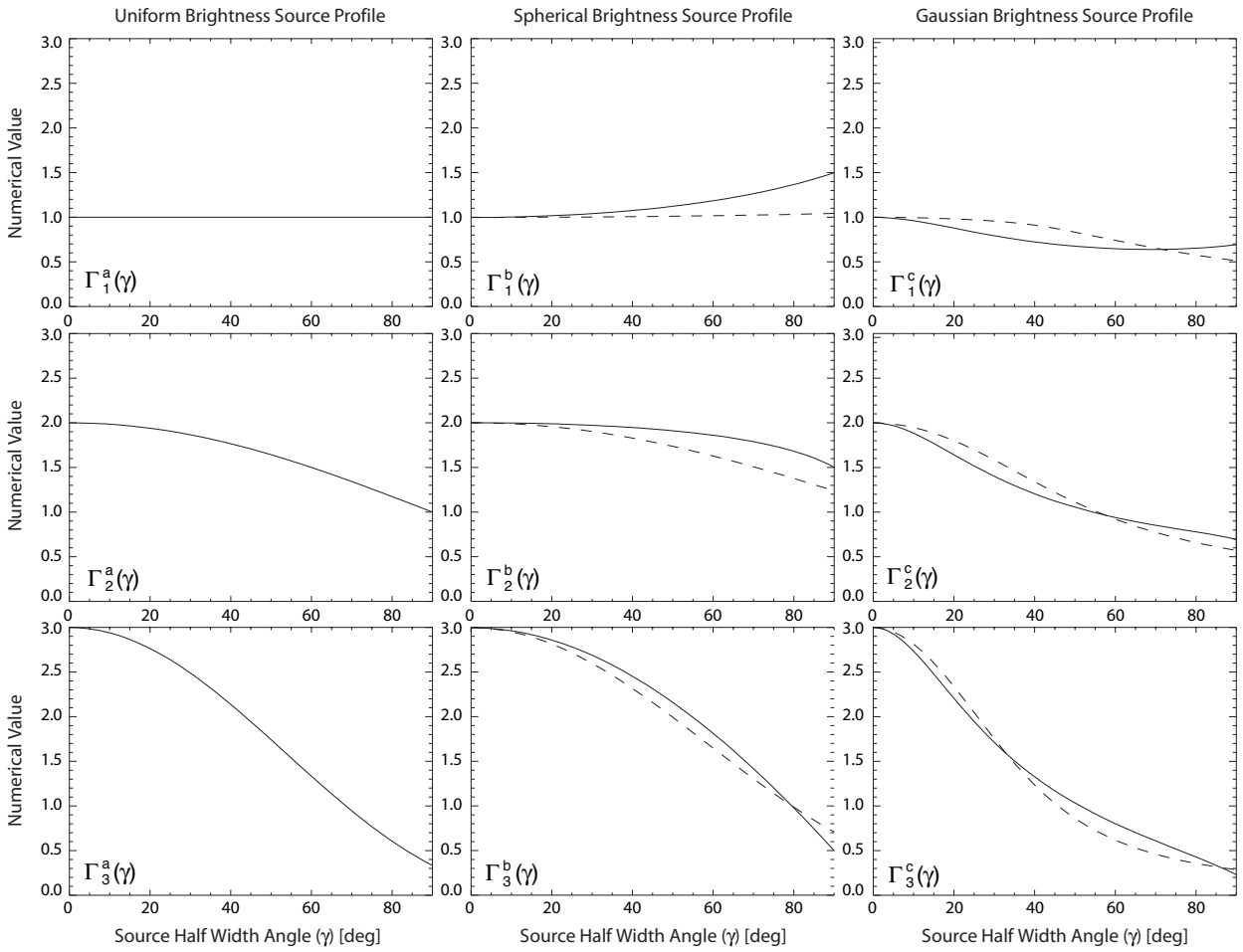

Figure 4: Normalized Γ_k^m coefficient as a function of the source half viewing width (γ). Coefficients for model (a), (b) and (c) are respectively shown in the 1st, 2nd and 3rd column. Coefficients of order $k = 1$, 2 and 3 are shown in row 1, 2 and 3, respectively. The coefficients were computed using the expressions with (dashed line, only for model (b) and (c)) or without (solid line) of small source approximation.

3 Errors induced by the source extension on GP results

Equation (33) gives the expression of the measurements recorded with dipole antennas in the case of an extended source with circular symmetry. We use below these expressions to evaluate the influence of the source size and radial profile on GP inversions that are assuming unresolved radio sources.

We study two GP inversions presented in paper 1. The "General Case Inversion", for which there is no assumption on the source (except that it is unresolved), is valid for $V \neq 0$. The "Circular polarization Case Inversion" is dedicated to sources with no linear polarization. For that second inversion, the case $V = 0$ is not singular. Both inversions require simultaneous measurements on three non coplanar antennas.

Following the method of paper 1, we simulate the receiver response induced by an extended source — i.e. using eq. (33) to model the measurements — and assume that these measurements were obtained with a point source (as in eq. 2) for the GP inversion. We test several source center directions in the spacecraft frame and several polarization states. As the flux density only appears as a multiplying factor for correlation measurements, we simulate our data with a single value $S_0 = 10^{-15}\, W m^{-2}\, Hz^{-1}$. We use the model antenna parameters used in paper 1, which are close to the actual ones of the Cassini/RPWS electrical antenna system. The three antennas are named $\vec{h}_{+X}$, $\vec{h}_{-X}$ and $\vec{h}_Z$. Their effective relative length, colatitude and azimuth in the spacecraft frame, are respectively: $h_{+X} = 1.0$, $\theta_{+X} = 110°$ and $\phi_{+X} = 20°$; $h_{-X} = 1.0$, $\theta_{-X} = 115°$ and $\phi_{-X} = 165°$; $h_Z = 0.8$, $\theta_Z = 30°$ and $\phi_Z = 90°$.

As in paper 1, we define β_{+XZ} (resp. β_{-XZ}) as the angular distance between the source direction and the plane formed by the $\vec{h}_{+X}$ (resp. $\vec{h}_{-X}$) and $\vec{h}_Z$ pair of antenna, and α_Z as the angular distance between the source direction and the $\vec{h}_Z$ antenna.

3.1 General Case Inversion

This inversion (see paper 1, section 2.1.1) uses three antenna measurements and solves for the full set of GP unknowns (S, Q, U, V, θ and ϕ). We have shown in paper 1 that the data selection necessary to get accurate measurements with this inversion is a Signal to Noise Ratio (SNR>23 dB) coupled with a geometrical selection $\beta_{\pm XZ} > 20°$, which also implies $\alpha_Z > 20°$. With these constraints, we achieve an accuracy of 1° on directions, 1 dB on flux densities and 10% on polarization measurements.

The simulation data sets were built with 2522 source directions (5° steps in azimuths and colatitudes) and 208 polarization states (excluding $V = 0$). Each run is computed with one of the three source profile models (a, b or c) and a given source size γ (1°, 2°, 5° or 10°). This gives thus a total of $2522 \times 208 = 524576$ simulated data points for each of the 12 ($= 3 \times 4$) runs.

The error levels are summarized in Table 1.

3.1.1 Source position determination

The GP inversion provides the colatitude θ and azimuth ϕ defining the direction of arrival of the incoming electromagnetic wave in the spacecraft frame. We define the error on the source determination as the angular distance between the true direction of the center of the simulated source (input values) and the resulting value given by the GP inversion (output values). This angular distance is noted $\Delta\xi$.

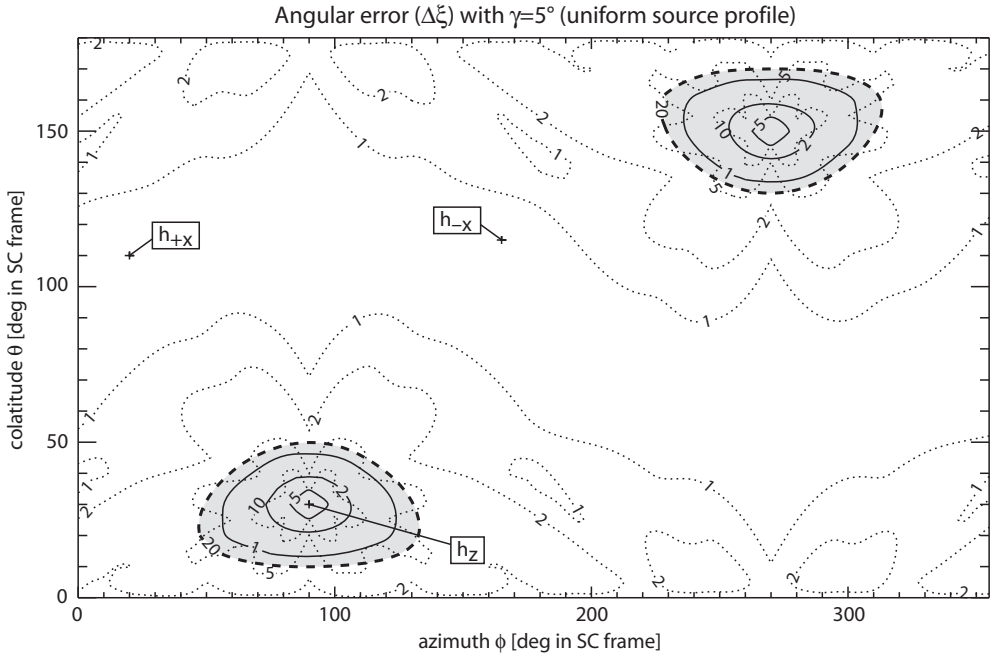

Figure 5: Angular Error on GP results using the "General Case Inversion", for an extended source with a $\gamma = 5°$ and an uniform brightness profile (model a). Isocontour lines are represented in the spacecraft frame spherical coordinates: colatitude θ and azimuth ϕ. The antenna directions are marked with + signs and labelled as in paper 1. The different isocontour lines are: mean angular error for a given direction (solid line); maximum angular error for a given direction (doted line); 20° distance from the h_Z antenna (thick dashed line + shaded region).

Fig. 5 displays the angular bias induced by an extended source with $\gamma = 5°$ with a uniform intensity profile (model a). The errors are deterministic and depend on both direction of arrival and polarization degree. The condition $\alpha_Z > 20°$ is consistent with a $\sim$1° average error and a $\sim$5° maximum error.

Fig. 6 summarizes the same results for different source angular half widths ($\gamma = 1$, 2, 5 and 10°). We have displayed the error probability levels on the source position. A 1% (50%, resp.) error probability level means that only 1% (50% resp.) of the simulated data points have an error greater than this value with the given angular selection threshold and the given source profile and angular width. Fig. 7 shows the same data but displaying the spherical (and gaussian) source profile error probability levels versus the uniform source profile error probability levels. This Fig. clearly shows that the error induced by a spherical profile source with an angular half width γ is equal to the one induced by a uniform profile source with an angular half width 0.80γ. The same statement can also be done with the gaussian profile source, equivalent to a 2.88 times larger uniform source profile. Comparing the actual angular biaises induced by the different models on the simulation grid, we observe that this also means that a spherical (or gaussian) profile source induces the same amount of angular bias on the source position as a uniform profile source with an angular width larger by the given factor.

3.1.2 Source polarization determination

The GP inversion provides the polarization state of the detected incoming electromagnetic wave in terms of two sets of three Stokes parameters (Q, U, V). Each set is computed using either the (h_{+X},h_Z) pair of antennas or the (h_{-X},h_Z) one. We only show the results obtained on the (h_{+X},h_Z) pair of antennas. We

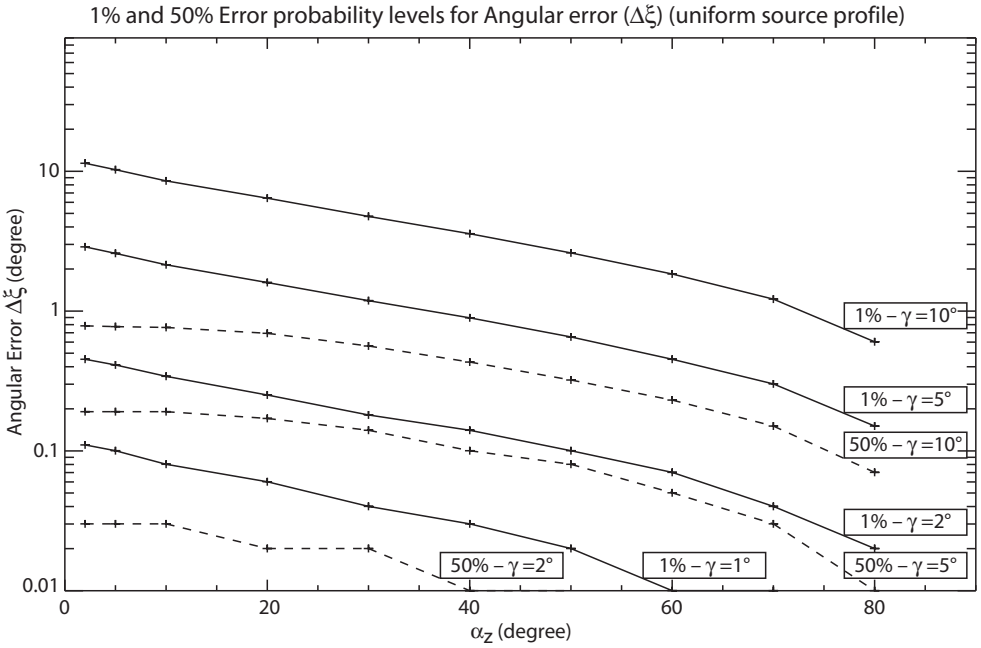

Figure 6: Error probability levels on the source position $\Delta\xi$ caused by an extended source using the "General Case Inversion". The error probability levels 1% and 50% are displayed versus the angular selection threshold α_Z, for an uniform brightness source (model a), and for several source angular width $\gamma = 1$, 2, 5 or 10°.

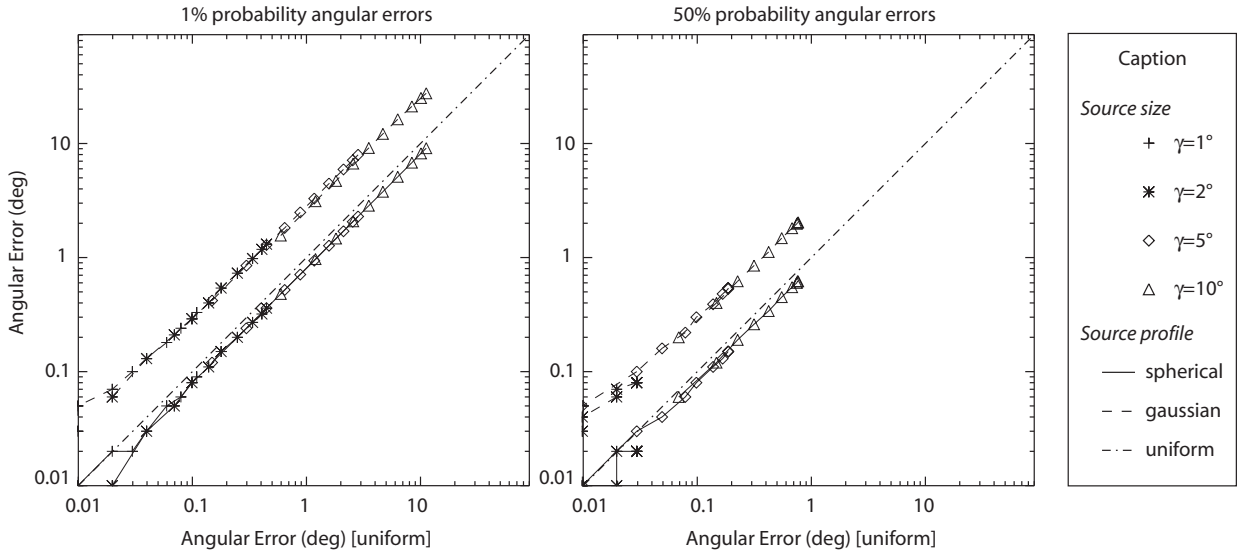

Figure 7: Comparison of the angular errors induced by the three different source profiles, for several angular thresholds and for two error probability levels (left: 50%, right: 1%). We used the angular error levels displayed in figure 6 and displayed the gaussian and spherical source profile results versus the uniform source profile ones. We observe that the error probability levels induced by a spherical (resp. gaussian) brightness distribution model is equivalent to the error probability levels induced by an uniform brightness distribution model with a radius 0.80γ (resp. 2.88γ).

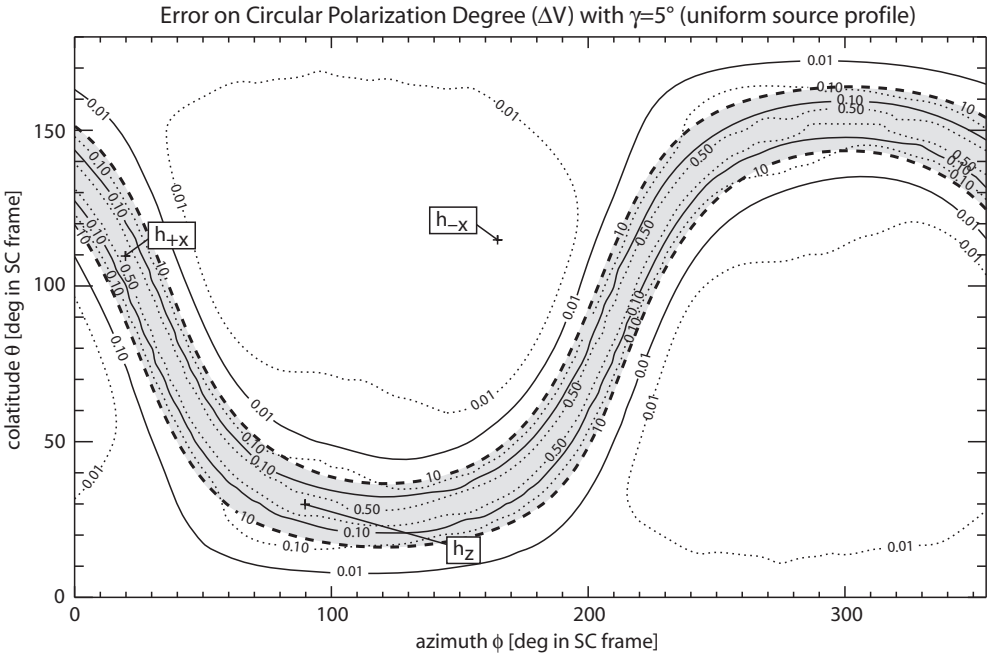

Figure 8: Circular polarization error on GP results using the "General Case Inversion", for an extended source with a $\gamma = 5°$, an uniform brightness profile (model a) and for the (h_{+X},h_Z) pair of antennas. Isocontour lines are represented in the spacecraft frame spherical coordinates: colatitude θ and azimuth ϕ. The antenna directions are marked with + signs and labelled as in paper 1. The different isocontour lines are: mean angular error for a given direction (solid line); maximum angular error for a given direction (doted line); 10° distance from the (h_{+X},h_Z) pair of antenna plane (thick dashed line).

show first the error on the circular polarization degree, noted ΔV, which is the absolute difference between the circular polarization degrees of the simulated incoming wave and the resulting value computed through the inversion. We then show the error on the linear polarization degree, noted ΔL, with $L = \sqrt{Q^2 + U^2}$.

Fig. 8 shows the error on the circular polarization degree induced by a extended source with $\gamma = 5°$ with a uniform intensity profile (model a). The $\beta_{+XZ} > 10°$ condition is consistent with a $\lesssim$10% average (and maximum) error. A $\beta_{+XZ} > 20°$ geometrical condition would be consistent for a $\sim$1% average accuracy. Fig. 9 summarizes the same results for different angular source widths ($\gamma = 1$, 2, 5 and 10°). This figure is interpreted as in Fig. 6 (see section 3.1.1). This figure shows that the absolute error on the circular polarization degree (1% error probability level) is typically less than 0.10 for β_{XZ}>10° with $\gamma = 5°$.

The same analysis has been done for the errors on the linear polarization degree (ΔL) and the results are very similar: the absolute error on the circular polarization degree (1% error probability level) is less than 0.10 for β_{XZ}>7.5° with $\gamma = 5°$. The 50% error probability level drops below 0.01 for β_{XZ}>7.5°, with $\gamma = 10°$.

3.1.3 Source flux determination

The error on the source flux determination (ΔS) are expressed in $dB[V^2/Hz]$, i.e. as a log scaled spectral power. The variations of ΔS are similar to the one presented on Fig. 8. Using the geometrical selection β_{XZ}>10° with $\gamma = 5°$, the 50% error probability level is 0.22 $dB[V^2/Hz]$, and the 1% level is below 0.01 $dB[V^2/Hz]$.

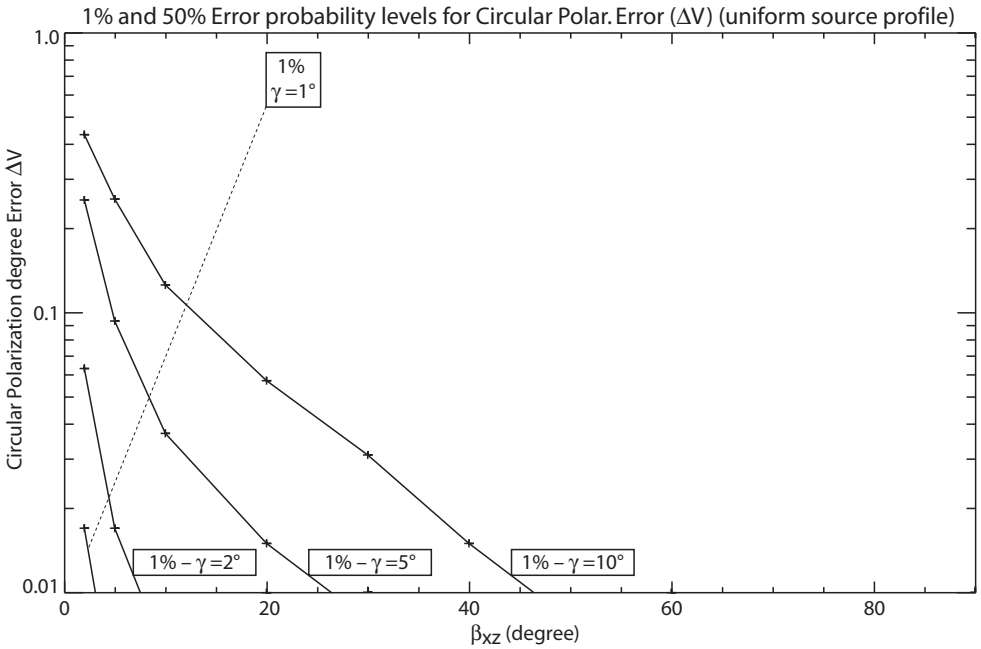

Figure 9: Error probability levels on the wave circular polarization degree ΔV caused by an extended source using the "General Case Inversion". The error probability levels are displayed versus the angular selection threshold β_{+XZ}, for an uniform brightness source model (model a), and for several source angular width $\gamma = 1$, 2, 5 or 10°. The 50% error probability levels are not displayed because they are lower than ΔV=0.01.

source size	$\Delta\xi$		ΔV		ΔL		$\Delta S^{(1)}$	
(γ)	1%	50%	1%	50%	1%	50%	1%	50%
1°	0.06°	<0.01°	<0.01	<0.01	<0.01	<0.01	<0.01	<0.01
2°	0.23°	0.02°	<0.01	<0.01	<0.01	<0.01	0.04	<0.01
5°	2.6°	0.18°	0.04	<0.01	0.05	<0.01	0.22	<0.01
10°	6.2°	0.7°	0.12	<0.01	0.18	<0.01	0.80	0.06

Table 1: Errors (1% and 50% error probability levels) for an extended source with an uniform brightness profile and the following angular selection: $\alpha_Z > 20°$ and $\beta_{XZ} > 10°$. (1) The error on the source flux determination ΔS is expressed in $dB[V^2/Hz]$

3.1.4 Final data selection

Table 1 summarizes the errors for different source sizes with an angular selection $\alpha_Z > 20°$ and $\beta_{XZ} > 10°$. This angular selection includes the selection given in paper 1, which was $\beta_{XZ} > 20°$. This latter criterion is required to get the following typical errors in case of a point source: $\Delta\xi < 1°$, $\Delta S < 1.0dB$, $\Delta L < 0.1$ and $\Delta V < 0.1$. The angular selection obtained in this study is providing the same order of magnitude of accuracy for flux and polarization parameters (ΔS, ΔL and ΔV) with a source half aperture $\gamma < 10°$, and for direction of arrival determinations with a source half aperture $\gamma < 5°$. As noted in Fig. 7 (and observed for ΔS, ΔV and ΔL also), the source profile only changes the error levels with a scaling factor supposing that a gaussian profile source is equivalent to the 2.88 (0.80 in case of a spherical source) times larger uniform source.

3.2 Circular Polarization Case Inversion

This inversion (see section 2.1.2 in paper 1) uses the three antenna measurements to solve the GP equations in case of a incoming wave that has no linear polarization (U=Q=0). The unknowns are then S, V, θ and ϕ. We showed in paper 1 that the data selection necessary to get accurate measurements with this inversion is a SNR selection (SNR>23 dB) coupled with a geometrical selection $\beta_{\pm XZ} > 20°$. A second geometrical selection was pointed out: $\alpha_Z < 50°$ taking into account the 8-bits digitization errors (as for the Cassini/RPWS radio receiver). In the case of a 12-bits digitalization scheme (as for the two STEREO/Waves radio receivers), this last selection is not useful. With the data selection mentioned, we can achieve an accuracy of 1° on directions, 1 dB on flux measurements and 10% on polarization measurements.

The simulation data sets was built with 9 circular polarization states (between -1 and 1, with 0.25-wide steps) and 10226 directions of arrival (2.5° steps in azimuths and colatitudes). Each run is computed with one of the three source profile models (a, b or c) and a given source size γ (1°, 2°, 5° or 10°). This gives thus a total of $9 \times 10226 = 92034$ simulated data points for each of the 12 ($= 3 \times 4$) runs.

3.2.1 Source position determination

As in section 3.1.1, we characterize the errors with $\Delta\xi$. Fig. 10 shows error level isocontours for the "Circular Polarization Case Inversion". The figure shows that the errors are larger along the antenna planes: mainly along the ($h_{\pm X}$,h_Z) planes and in a smaller extent along the (h_{+X},h_{-X}) plane. With $\beta_{XZ} > 10°$, the 1% angular error probability level is lower than 2° for $\gamma < 5°$, and the 50% error probability level is lower than 1° for $\gamma < 10°$. With a more restricted angular selection ($\beta_{XZ} > 22°$), we get $\Delta\xi$ lower than $\sim 1°$ for $\gamma < 10°$ (at the 1% error probability level). Note that the latter selection is removing the area situated between the $(+X, Z)$ and $(-X, Z)$ antenna planes where the error amplitudes are higher (see Fig. 10).

3.2.2 Source polarization determination

We are supposing here that the source has no linear polarization (i.e. Q=0 and U=0). The circular polarization error on GP results using this inversion is similar to the ones presented on Fig. 8 for the general case inversion. With $\beta_{XZ} > 10°$, the 1% error probability level is lower than 0.12 for any $\gamma < 10°$.

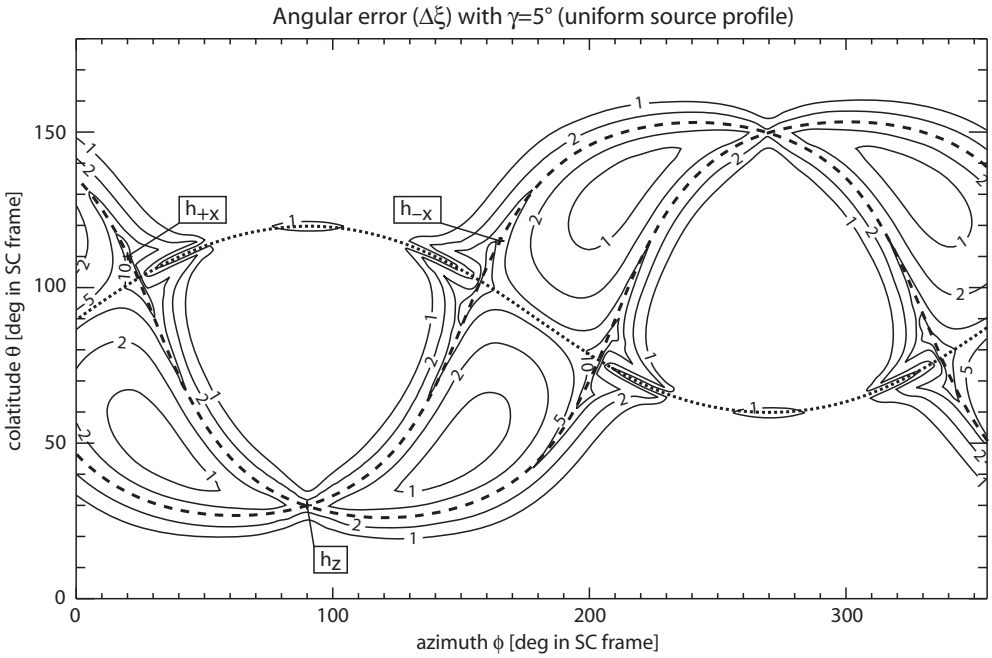

Figure 10: Angular Error on GP results using the "Circular Polarization Inversion", for an extended source with a $\gamma = 5^\circ$ and an uniform brightness profile (model a). Isocontour lines are represented in the spacecraft frame spherical coordinates: colatitude θ and azimuth ϕ. The antenna directions are marked with $+$ signs and labelled as in paper 1. The solid lines are maximum angular error isocontours for a given direction. The thick dashed lines show the direction within the antenna planes (h_Z and $h_{\pm X}$); these set of directions correspond to $\beta_{\pm XZ} = 0$. The thick dotted line is the direction perpendicular to the h_Z antenna ($\alpha_Z = 90^\circ$).

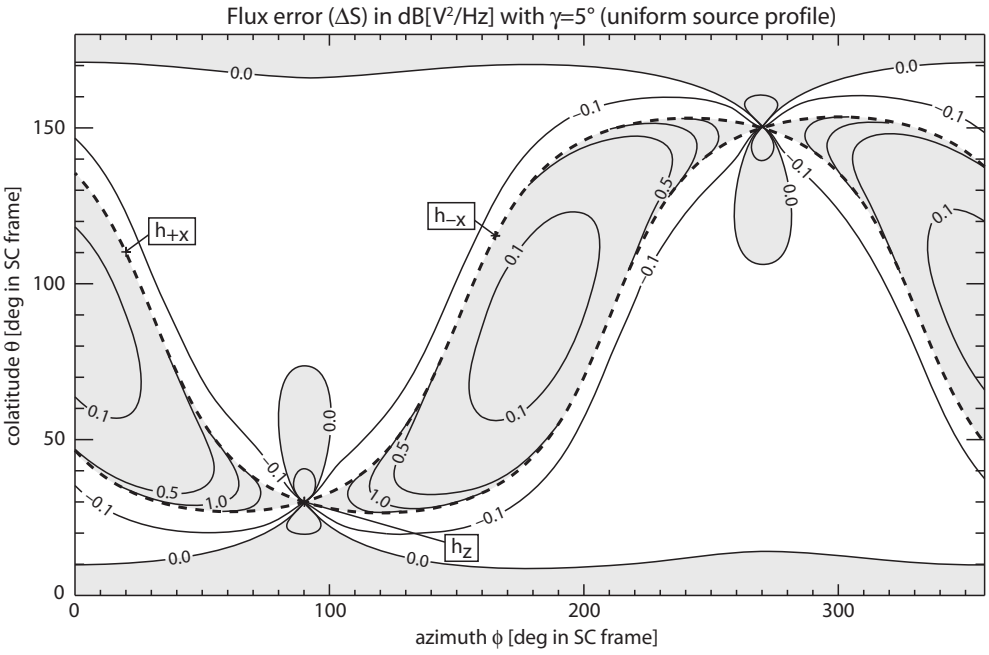

Figure 11: Flux Error on GP results using the "Circular Polarization Inversion", for an extended source with a $\gamma = 5°$ and an uniform brightness profile (model a). Flux density errors are in $dB[V^2/Hz]$. Isocontour lines are represented in the spacecraft frame spherical coordinates: colatitude θ and azimuth ϕ. The antenna directions are marked with + signs and labelled as in paper 1. The solid lines are maximum angular error isocontours for a given direction. The thick dashed lines show the direction within the antenna planes (i.e. the directions corresponding to $\beta_{\pm XZ} = 0$). The grey shaded areas correspond to the positive error areas (measured flux greater than actual flux), the white ones are the negative ones.

source size	$\Delta\xi$		ΔV		$\Delta S^{(1)}$	
(γ)	1%	50%	1%	50%	1%	50%
1°	<0.1°	<0.1°	<0.01	<0.01	<0.01	<0.01
2°	0.3°	<0.1°	<0.01	<0.01	0.03	<0.01
5°	2.0°	0.2°	0.04	<0.01	0.19	0.01
10°	7.1°	0.9°	0.12	<0.01	0.66	0.03

Table 2: Typical errors (1% and 50% error probability levels) for an extended source with an uniform brightness profile and an angular selection $\beta_{XZ} > 10°$. (1) The error on the source flux determination ΔS is expressed in $dB[V^2/Hz]$

3.2.3 Source flux determination

The error on the flux determination are shown on Fig. 11 for $\gamma = 5°$ and a uniform source profile. This figure shows that strong errors occur along the antenna planes — i.e. the planes (h_Z,h_{+X}) and (h_Z,h_{-X}) — and close to the h_Z antenna direction. With 10°, we restrict the error levels below $\Delta S > 1dB[V^2/Hz]$. Table 2 shows the 1% and 50% error probability levels.

3.2.4 Final data selection

Table 2 summarizes the error levels for different source sizes with a typical angular selection $\beta_{XZ} > 10°$. This angular selection is less constraining than the selection given in paper 1, which was $\beta_{XZ} > 20°$ and $\alpha_Z < 50°$. This latter criterium is required to get the following typical errors in case of a point source: $\Delta\xi < 1°$, $\Delta S < 1.0dB$ and $\Delta V < 0.1$. The angular selection obtained in this study is providing the same order of magnitude of accuracy for flux and polarization parameters (ΔS, ΔL and ΔV) with a source half aperture $\gamma < 10°$, and for direction of arrival determinations with a source half aperture $\gamma < 5°$.

4 Discussion

We have obtained the expressions of measurements (auto- and cross-correlation of the voltages measured on two antennas) taking into account the size of the source with different radial brightness distribution profiles, given its disk-equivalent radius. The general expression is proposed in Eq. (33). We have checked that in case of $\gamma = 0$ the expressions are identical to the ones published in previous studies [*Lecacheux*, 1978; *Ladreiter et al.*, 1995,paper 1]. We also checked expression (33) against the previous results on extended source GP published by *Manning and Fainberg* [1980]. Although their formulas were obtained in a special case (auto-correlation only with perpendicular antennas on a spinning spacecraft), we obtain the same expressions (see appendix A). The expressions have been formulated here for three different radial intensity profiles (uniform, spherical and gaussian). Any other radial intensity profile can be studied numerically.

We have studied in this paper the case of an axisymmetric source, assuming that any extended source could be represented by its disk-equivalent source. We numerically computed the correlation response for elliptical sources with uniform brightness and polarization degrees distributions. This study allowed us to check that an uniform elliptical source induce the same voltage correlation than the uniform circular source which subtends the same solid angle, ensuring the validity of our assumption.

We have shown that the errors on the results of the analytical GP inversions presented in paper 1 are within

the error bars of these inversions, given a geometrical selection (which includes the geometrical selection proposed in paper 1) and a disk-equivalent radius of the source below 5° for directions and 10° for flux and polarization. The error levels are given in Tables 1 and 2. As shown in Fig. 7, the radial intensity profile of the source only modifies the amplitude of the final error on GP with a scaling factor: a gaussian source (resp. spherical) induces errors equivalent to a 2.88 (resp. 0.80) times larger uniform source. Any other source profile might be studied but they are likely to show the same behaviour.

The implications of this study on the scientific results obtained with point source inversions are different depending on the observed source. In the case of the Saturn (observed with Cassini), the closest Saturn flyby of Cassini occurred during the insertion orbit at ∼1.3 R_S (Saturn radii, 1 R_S=60,268 km). At this distance a 5° source is approximately 6800 km ($0.11 R_S$). There is no estimate of the size of the radio sources at Saturn. *Cowley et al.* [2004] gave an estimation for the width of the UV aurora active region at Saturn of 500–1000 km width. This gives the typical width the region in which the auroral radio emission may occur. However the radio emission beaming pattern is not isotropic but probably has the shape of a hollow cone [*Zarka*, 1998]. The radio emission are also very bursty and sporadic. It is then unlikely that a spacecraft will be within the emission beam of several contiguous sources. The point source hypothesis is thus valid in the case of Saturn's auroral radio emissions. In the case of solar radio bursts, *Steinberg et al.* [1985] showed that the typical angular extension of type III bursts is of the order of 30° at 100 kHz when observed from the Earth. This angular extension is induced by scattering. The point source GP inversions may then give erroneous results. A GP inversion providing the size of the source thus is necessary to characterize correctly the solar radio bursts with the STEREO/Waves experiments.

A full GP inversion providing the size of the source requires the inversion of the GP measurements system for directions (θ, ϕ), flux (S), polarization (Q, U, V) and disk-equivalent radius of the source (γ), i.e. inverting a system of 7 (3 auto- and 2 complex cross-correlations, as for the Cassini data) or 9 (3 auto- and 3 complex cross-correlations, as for the STEREO data) measurements for 7 unknowns. As the system is degenerated — it is not possible to obtain separately direction and polarization, see paper 1 — it might not be possible to obtain the full set of GP unknowns as a result in the case where we have only 7 measurements. Assumptions on different parameters would however help inverting the system in that case (for instance: giving the position of the source center or supposing that the source has no polarization or is purely circularly polarized). This means that only the STEREO data might be able to be used to do full GP inversions including the size of the source. If no analytical direct inversion is found, it may be built on a minimization process [see *Ladreiter et al.*, 1995; *Santolík et al.*, 2003; *Vogl et al.*, 2004] and will be described in a future paper. The present study however characterize the limits of the GP inversions derived in paper 1 in case of an extended radio source. Finally, this study can also be used for the future JUNO mission (jovian polar orbiter with perijoves $< 5000 km$). If this spinning spacecraft has a GP radio receiver onboard, it will provide radio source localization with an accuracy of a few 100 km, close to that obtained with the UV images from the Hubble Space Telescope (1 pixel is about 200 km).

Acknowledgement

The author was supported by the CNES (Centre National d'Études Spatiales) through a Post-Doctoral fellowship. The author would like to thank P. Zarka, M. Maksimovic and S. Hoang for their helpful suggestions and discussions, as well as Jean-Louis Bougeret, Principal Investigator of the STEREO/Waves experiment.

A Checking equation (33) with *Manning and Fainberg* [1980] results

Manning and Fainberg [1980] provided an equation set to solve the problem in the particular case of a spinning spacecraft. In addition the two antennas considered were supposed to be either axial ($\theta_{//} = 0$) or equatorial ($\theta_{\perp} = \pi/2$) and they only computed the spectral power on one antenna at a time (autocorrelation only). Our expressions are valid whatever the antenna direction is. We check here their consistency with *Manning and Fainberg* [1980] ones.

Equation (33) gives us the general expression of the spectral power measured by dipole antennas in the case of an extended source. As *Manning and Fainberg* [1980] made the assumption that the source was uniform, we can rewrite equation (33) using model a, in the case of the autocorrelation on the ith antenna:

$$\begin{aligned} P_{ii} &= \frac{Z_0\, G h_i^2\, S_0}{2}\left[(1+Q)\left(A_i^2\frac{1+\cos\gamma}{2}+C_i^2\frac{1-\cos\gamma}{2}\right)+2U\left(A_iB_i\frac{1+\cos\gamma}{2}\right)\right. \\ &\quad +(1-Q)\left(A_i^2\frac{1}{2}\left(-\cos\gamma+\frac{1+\cos\gamma+\cos^2\gamma}{3}\right)\right. \\ &\quad\quad +B_i^2\frac{1}{2}\left(1+\frac{1+\cos\gamma+\cos^2\gamma}{3}\right) \\ &\quad\quad \left.\left.\left.+C_i^2\left(\frac{1+\cos\gamma}{2}-\frac{1+\cos\gamma+\cos^2\gamma}{3}\right)\right)\right)\right] \end{aligned} \tag{48}$$

In the case of an axial dipole, we have $\theta_{//} = 0$ and $\phi_{//} = 0$. This implies that $A_{//} = \sin\theta_C$, $B_{//} = 0$ and $C_{//} = \cos\theta_C$. We then get $P_{//}$ as follows:

$$\begin{aligned} P_{//} &= \frac{Z_0\, G h_{//}^2\, S_0}{2}\left[(1+Q)\left(\sin^2\theta_C\frac{1+\cos\gamma}{2}+\cos^2\theta_C\frac{1-\cos\gamma}{2}\right)\right. \\ &\quad +(1-Q)\left(\sin^2\theta_C\frac{1}{2}\left(-\cos\gamma+\frac{1+\cos\gamma+\cos^2\gamma}{3}\right)\right. \\ &\quad\quad \left.\left.+\cos^2\theta_C\left(\frac{1+\cos\gamma}{2}-\frac{1+\cos\gamma+\cos^2\gamma}{3}\right)\right)\right] \end{aligned} \tag{49}$$

Defining $\Delta = \cos\gamma + \cos^2\gamma$, $P_{//}$ rewrites:

$$\begin{aligned} P_{//} &= Z_0\, G h_{//}^2\, S_0\left[\frac{1}{3}+\frac{\Delta}{12}(1-3\cos^2\theta_C)+\frac{Q}{12}\big(2-\Delta(1-3\cos^2\theta_C)\right. \\ &\quad \left.-6\cos\gamma\cos 2\theta_C\big)\right] \end{aligned} \tag{50}$$

In the case of an equatorial dipole, we then have $\theta_{\perp} = \pi/2$. This leads to $A_{\perp} = -\cos\theta_C\cos(\phi_C - \phi_{\perp})$,

$B_\perp = -\sin(\phi_C - \phi_\perp)$ and $C_\perp = \sin\theta_C \cos(\phi_C - \phi_\perp)$. We then get $P_\perp$ as follows:

$$\begin{aligned} P_\perp &= \frac{Z_0\, G h_\perp^2\, S_0}{2}\left[(1+Q)\left(\cos^2\theta_C\cos^2(\phi_C-\phi_\perp)\frac{1+\cos\gamma}{2}+\sin^2\theta_C\cos^2(\phi_C-\phi_\perp)\frac{1-\cos\gamma}{2}\right)\right. \\ &\quad +2U\left(\cos\theta_C\cos(\phi_C-\phi_\perp)\sin(\phi_C-\phi_\perp)\frac{1+\cos\gamma}{2}\right) \\ &\quad +(1-Q)\left(\cos^2\theta_C\cos^2(\phi_C-\phi_\perp)\frac{1}{2}\left(-\cos\gamma+\frac{1+\cos\gamma+\cos^2\gamma}{3}\right)\right. \\ &\quad\quad +\sin^2(\phi_C-\phi_\perp)\frac{1}{2}\left(1+\frac{1+\cos\gamma+\cos^2\gamma}{3}\right) \\ &\quad\quad \left.\left.+\sin^2\theta_C\cos^2(\phi_C-\phi_\perp)\left(\frac{1+\cos\gamma}{2}-\frac{1+\cos\gamma+\cos^2\gamma}{3}\right)\right)\right] \end{aligned} \tag{51}$$

Using the previously defined Δ notation and setting $\phi_A = \phi_C - \phi_\perp$, $P_\perp$ rewrites:

$$\begin{aligned} P_\perp &= Z_0\, G h_\perp^2\, S_0\left[\frac{1}{3}-\frac{\Delta}{24}(1-3\cos^2\theta_C)-\frac{Q}{24}(2-\Delta(1-3\cos^2\theta_C)-6\cos^2\theta_C\cos\gamma)\right. \\ &\quad +\frac{\sin 2\phi_A}{4}U\cos\theta_C(1+\cos\gamma) \\ &\quad \left.-\frac{\cos 2\phi_A}{8}\left(\Delta\sin^2\theta_C-Q(2+2\cos^2\theta_C\cos\gamma+\Delta\sin^2\theta_C)\right)\right] \end{aligned} \tag{52}$$

If we compare respectively equations (50) and (52) to equations (21) and (22) from *Manning and Fainberg* [1980], we get the exact same expressions.

References

Cecconi, B., and P. Zarka, Direction finding and antenna calibration through analytical inversion of radio measurements performed using a system of 2 or 3 electric dipole antennas, *Radio Sci.*, *40*, RS3003, doi: 10.1029/2004RS003070, 2005.

Cowley, S. W. H., E. J. Bunce, and R. Prangé, Saturn's polar ionospheric flows and their relation to the main auroral oval, *Ann. Geophys.*, *22*, 1379–1394, 2004.

Gurnett, D. A., et al., The Cassini radio and Plasma wave science investigation, *Space Sci. Rev.*, *114* (1–4), 395–463, doi:10.1007/s11214-004-1434-0, 2004.

Kaiser, M. L., The STEREO mission: an overview, *Adv. Space. Res.*, *36*, 1483–1488, doi: 10.1016/j.asr.2004.12.066, 2005.

Kraus, J. D., *Radio Astronomy*, McGraw-Hill, New York, 1966.

Ladreiter, H. P., P. Zarka, and A. Lecacheux, Direction finding study of Jovian hectometric and broadband kilometric radio emissions: Evidence for their auroral origin, *Planet. Space Sci.*, *42*, 919–931, 1994.

Ladreiter, H. P., P. Zarka, A. Lecacheux, W. Macher, H. O. Rucker, R. Manning, D. A. Gurnett, and W. S. Kurth, Analysis of electromagnetic wave direction finding performed by spaceborne antennas using singular-value decomposition techniques, *Radio Sci.*, *30*, 1699–1712, 1995.

Lecacheux, A., Direction Finding of a Radiosource of Unknown Polarization with Short Electric Antennas on a Spacecraft, *Astron. Astrophys.*, *70*, 701–706, 1978.

Manning, R., Insrumentation For Space-Based Low Frequency Radio Astronomy, in *Radio Astronomy at Long Wavelengths*, *Geophysical Monograph*, vol. 119, edited by R. G. Stone, K. W. Weiler, M. L. Goldstein, and J.-L. Bougeret, pp. 329–337, AGU, Washington DC, 2000.

Manning, R., and J. Fainberg, A new method of measuring radio source parameters of a partially polarized distributed source from spacecraft observations, *Space Sci. Inst.*, *5*, 161–181, 1980.

Oswald, T., W. Macher, G. Fischer, H. O. Rucker, J.-L. Bougeret, M. L. Kaiser, and K. Goetz, Numerical analysis of the STEREO/Waves antennas: First results, in *Planetary Radio Emissions VI*, edited by H. O. Rucker, W. S. Kurth, and G. Mann, pp. 475–482, Austrian Acad. Sci. Press, Graz, Austria, 2006.

Rucker, H. O., W. Macher, G. Fischer, T. Oswald, J.-L. Bougeret, M. L. Kaiser, and K. Goetz, Analysis of spacecraft antenna systems: Implications for STEREO/WAVES, *Advances in Space Research*, *36*, 1530–1533, doi:10.1016/j.asr.2005.07.060, 2005.

Santolík, O., M. Parrot, and F. Lefeuvre, Singular value decomposition methods for wave propagation analysis, *Radio Sci.*, *38*(1), 1010, doi:10.1029/2000RS002523, 2003.

Steinberg, J.-L., S. Hoang, and G. A. Dulk, Evidence of scattering effects on the sizes of interplanetary Type III radio bursts, *Astron. Astrophys.*, *150*, 205–216, 1985.

Vogl, D. F., et al., In–flight calibration of the Cassini-Radio and Plasma Wave Science (RPWS) antenna system for direction-finding and polarization measurements, *J. Geophys. Res.*, *109*, A09S17, doi: 10.1029/2003JA010261, 2004.

Zarka, P., Auroral radio emissions at the outer planets: Observations and theories, *J. Geophys. Res.*, *103*, 20,159–20,194, 1998.

Zarka, P., B. Cecconi, and W. S. Kurth, Jupiter's low-frequency radio spectrum from Cassini/Radio and Plasma Wave Science (RPWS) absolute flux density measurements, *J. Geophys. Res.*, *109*, A09S15, doi: 10.1029/2003JA010260, 2004.